

Article

Carbon Isotope Fractionation during the Formation of CO₂ Hydrate and Equilibrium Pressures of ¹²CO₂ and ¹³CO₂ Hydrates

Hiromi Kimura ¹, Go Fuseya ¹, Satoshi Takeya ² and Akihiro Hachikubo ^{3,*}

¹ Kitami Institute of Technology, Graduate School of Engineering, 165 Koen-cho, Kitami 090-8507, Japan; mayu011970@gmail.com (H.K.); fuseya1992@gmail.com (G.F.)

² National Metrology Institute of Japan (NMIJ), National Institute of Advanced Industrial Science and Technology (AIST), Central 5, Higashi 1-1-1, Tsukuba 305-8565, Japan; s.takeya@aist.go.jp

³ Environmental and Energy Resources Research Center, Kitami Institute of Technology, 165 Koen-cho, Kitami 090-8507, Japan

* Correspondence: hachi@mail.kitami-it.ac.jp

Abstract: Knowledge of carbon isotope fractionation is needed in order to discuss the formation and dissociation of naturally occurring CO₂ hydrates. We investigated carbon isotope fractionation during CO₂ hydrate formation and measured the three-phase equilibria of ¹²CO₂-H₂O and ¹³CO₂-H₂O systems. From a crystal structure viewpoint, the difference in the Raman spectra of hydrate-bound ¹²CO₂ and ¹³CO₂ was revealed, although their unit cell size was similar. The δ¹³C of hydrate-bound CO₂ was lower than that of the residual CO₂ (1.0–1.5‰) in a formation temperature ranging between 226 K and 278 K. The results show that the small difference between equilibrium pressures of ~0.01 MPa in ¹²CO₂ and ¹³CO₂ hydrates causes carbon isotope fractionation of ~1‰. However, the difference between equilibrium pressures in the ¹²CO₂-H₂O and ¹³CO₂-H₂O systems was smaller than the standard uncertainties of measurement; more accurate pressure measurement is required for quantitative discussion.

Keywords: CO₂ hydrate; carbon isotope; isotopic fractionation; phase equilibrium; Raman spectra



Citation: Kimura, H.; Fuseya, G.; Takeya, S.; Hachikubo, A. Carbon Isotope Fractionation during the Formation of CO₂ Hydrate and Equilibrium Pressures of ¹²CO₂ and ¹³CO₂ Hydrates. *Molecules* **2021**, *26*, 4215. <https://doi.org/10.3390/molecules26144215>

Academic Editors: Nobuo Maeda, Zhiyuan Wang and Xiaodong Shen

Received: 11 June 2021

Accepted: 7 July 2021

Published: 11 July 2021

Publisher's Note: MDPI stays neutral with regard to jurisdictional claims in published maps and institutional affiliations.



Copyright: © 2021 by the authors. Licensee MDPI, Basel, Switzerland. This article is an open access article distributed under the terms and conditions of the Creative Commons Attribution (CC BY) license (<https://creativecommons.org/licenses/by/4.0/>).

1. Introduction

Gas hydrates are crystalline clathrate compounds that have guest gas molecules encapsulated in hydrogen-bonded water cages and can be thermodynamically stable at high pressures and low temperatures. The phase equilibrium pressure-temperature conditions vary depending on the guest molecule type [1]. Gas hydrates with encapsulated natural gases exist in sub-marine/sublacustrine sediments and below the permafrost on Earth. Because they contain copious amounts of greenhouse gases, such as methane, concerns arose that their dissociation could add to global warming [2–4]. Hydrate-bound gas contains both hydrocarbons and CO₂ [5–7], and natural gas hydrates encapsulating CO₂ have been observed at the venting sites of liquid CO₂ [8,9]. On the other hand, the possibility of existing CO₂ hydrates on Mars was proposed [10,11] and the conditions for CO₂ hydrate formation on Mars have been discussed [12]. As above, CO₂ hydrates are critical in both geochemistry and space science and require better understanding.

Since CO₂ comprises carbon and oxygen atoms, several isotopic species of CO₂ exist, depending on the combination of stable isotopes (isotopologues: ¹²C, ¹³C, ¹⁶O, ¹⁷O, and ¹⁸O). For example, the abundance ratio of ¹³CO₂ is ~1.1% of the total CO₂ and the rest is almost ¹²CO₂. Stable isotope fractionation of the guest gas during the gas hydrate formation provides information for discussing the formation, maintenance, and decomposition processes of gas hydrates. For example, the trend of hydrogen and carbon isotope fractionation during the formation of synthetic methane and ethane hydrates was

investigated [13]. Moreover, the results were applied to estimate the formation process of natural gas hydrates [14–16]. Carbon isotope fractionation during the formation of CO₂ hydrates was reported [17], revealing that the CO₂ δ¹³C in the hydrate phase was 0.9‰ lower than that in the gas phase at 268 K [17]. Therefore, ¹²CO₂ is more easily encapsulated in the hydrate phase than ¹³CO₂. Because the temperature of existing natural gas hydrates at sea/lake bottom sediments is above 273 K, information about carbon isotope fractionation above the freezing point of water is needed to discuss the formation and dissociation of naturally occurring CO₂ hydrates. Furthermore, CO₂ hydrates have been suggested outside of Earth. Therefore, it is also necessary to confirm isotope fractionation in a wider temperature range.

In studies on methane hydrates, the equilibrium pressures of CH₃D and CD₄ hydrates were ~0.04 MPa and ~0.14 MPa higher than those of the CH₄ hydrate, respectively [18]. Because guest molecules, which have lower equilibrium pressure, are preferentially encapsulated in the gas hydrate cages, the difference in equilibrium pressures of CH₃D and CH₄ hydrates can explain the hydrogen isotope fractionation in methane during methane hydrate formation [18]. Thus, comparing the phase equilibrium *p*–*T* conditions of each gas hydrate encapsulating isotopologues can explain the trend of isotopic fractionation of guest gases during gas hydrate formation. However, the equilibrium pressure of ¹³CO₂ hydrates has not been reported.

In this study, we synthesized gas hydrate samples, encapsulated CO₂ isotopologues (¹²CO₂ and ¹³CO₂), and characterized their crystallographic properties using powder X-ray diffraction (PXRD) and Raman spectroscopy. We also measured the equilibrium pressures of ¹²CO₂ and ¹³CO₂ hydrates at a temperature range between 269 K and 278 K. We investigated carbon isotope fractionation between hydrate-bound gas and residual gas in a pressure cell in the temperature range of 226 K to 278 K.

2. Results and Discussion

We confirmed the crystallographic structures of ¹²CO₂ and ¹³CO₂ hydrates and obtained their lattice constants using the PXRD method. The diffraction patterns of cubic structure I (sI) hydrates were observed from these hydrates (Figure S1). The lattice constants of ¹²CO₂ and ¹³CO₂ hydrates were similar at 11.8352(6) Å and 11.8323(5) Å, respectively.

Figure 1 shows the Raman spectra of ¹²CO₂ and ¹³CO₂ hydrates and Table 1 summarizes the observed Raman shifts of hydrate-bound isotopologue CO₂ and their assignments to the vibrational modes. Two distinct peaks corresponding to the Fermi dyad of CO₂ in the hydrate cages were observed at 1278.2 cm^{−1} and 1381.9 cm^{−1} for ¹²CO₂ hydrates, corresponding to [19–21]. These peaks shifted to 1256.4 cm^{−1} and 1365.8 cm^{−1} for the ¹³CO₂ hydrate. Qin and Kuhs [21] observed 1366.6 ± 4.0 cm^{−1} for the upper Fermi dyad of hydrate-bound ¹³CO₂, and our data were consistent with their results. Definite differences (22 cm^{−1} and 16 cm^{−1} for lower and upper peaks, respectively) were found between these Raman peaks caused by the encapsulated ¹²CO₂ and ¹³CO₂ molecules.

Table 1. Observed Raman shifts of hydrate-bound CO₂ and assignments to the vibrational modes.

Guest Molecule	Raman Shift Gas/cm ^{−1}	Raman Shift Hydrate/cm ^{−1}	Assign	Vibrational Mode
¹² CO ₂	1285.40 [22]	1278.2 ^a , 1277 [19], 1278 [20], 1275.5 ± 0.8 [21]	ν ₁ + 2ν ₂ ^b	CO s-stretch + bend ^b
	1388.15 [22]	1381.9 ^a , 1381 [19], 1382 [20], 1379.4 ± 0.8 [21]		
¹³ CO ₂	1266.03 [22]	1256.4 ^a		
	1369.90 [22]	1365.8 ^a , 1366.6 ± 4.0 [21]		

^a This work, uncertainty is <1.1 cm^{−1}. ^b Fermi resonance.

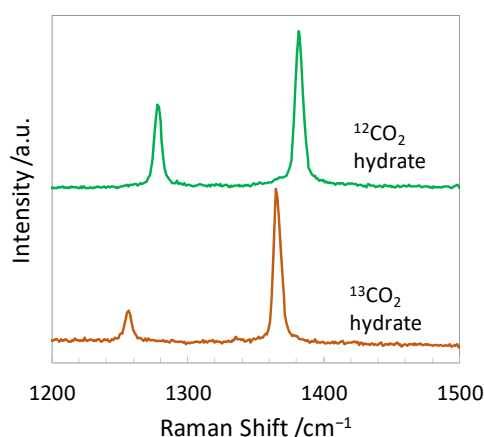


Figure 1. Raman spectra of $^{12}\text{CO}_2$ and $^{13}\text{CO}_2$ hydrates in the CO stretching vibration mode region of CO_2 . The spectra were recorded at atmospheric pressure and 140 K. (a.u., arbitrary units).

Table 2 lists and Figure 2 plots the p - T data for the three-phase equilibrium (ice/water + hydrate + vapor) for the $^{12}\text{CO}_2$ - H_2O and $^{13}\text{CO}_2$ - H_2O systems. The phase in the equilibrium of each point in Table 2 was determined using the quadruple point of the $^{12}\text{CO}_2$ - H_2O system (1.04 MPa and 271.6 K) reported by [23]. To ensure the accuracy of the experimental apparatus described in the previous section, we evaluated the equilibrium p - T data of $^{12}\text{CO}_2$ hydrates. From Figure 2, they correlate well with the literature [23–26]. The equilibrium pressures in the $^{13}\text{CO}_2$ - H_2O system are higher by 0.007–0.012 MPa compared with the corresponding values in the $^{12}\text{CO}_2$ - H_2O system between 269 K and 278 K. However, these differences are within the range of uncertainty of the pressure measurements.

Table 2. Three-phase equilibrium p - T conditions in $^{12}\text{CO}_2$ - H_2O and $^{13}\text{CO}_2$ - H_2O systems ^a.

T/K	$p_{^{12}\text{CO}_2\text{-H}_2\text{O}}/\text{MPa}$	$p_{^{13}\text{CO}_2\text{-H}_2\text{O}}/\text{MPa}$	Phase in Equilibrium
269.47	0.953	0.963	ice + hydrate + vapor
269.67	0.960	0.969	ice + hydrate + vapor
269.88	0.967	0.977	ice + hydrate + vapor
270.08	0.973	0.984	ice + hydrate + vapor
270.28	0.980	0.990	ice + hydrate + vapor
270.47	0.987	0.999	ice + hydrate + vapor
270.67	0.994	1.004	ice + hydrate + vapor
270.88	1.002	1.011	ice + hydrate + vapor
271.08	1.009	1.018	ice + hydrate + vapor
271.28	1.016	1.025	ice + hydrate + vapor
271.48	1.023	1.031	ice + hydrate + vapor
271.67	1.034	1.043	water + hydrate + vapor
271.88	1.058	1.067	water + hydrate + vapor
272.08	1.083	1.092	water + hydrate + vapor
272.28	1.109	1.118	water + hydrate + vapor
272.46	1.133	1.142	water + hydrate + vapor
272.66	1.159	1.168	water + hydrate + vapor
272.86	1.185	1.195	water + hydrate + vapor
273.05	1.212	1.223	water + hydrate + vapor
273.25	1.240	1.251	water + hydrate + vapor
273.45	1.270	1.280	water + hydrate + vapor
273.66	1.302	1.312	water + hydrate + vapor
273.85	1.333	1.342	water + hydrate + vapor
274.05	1.365	1.376	water + hydrate + vapor
274.26	1.397	1.408	water + hydrate + vapor
274.47	1.427	1.435	water + hydrate + vapor
274.67	1.461	1.469	water + hydrate + vapor

Table 2. Cont.

T/K	$p_{12\text{CO}_2\text{-H}_2\text{O}}/\text{MPa}$	$p_{13\text{CO}_2\text{-H}_2\text{O}}/\text{MPa}$	Phase in Equilibrium
274.87	1.496	1.504	water + hydrate + vapor
275.07	1.534	1.542	water + hydrate + vapor
275.27	1.569	1.578	water + hydrate + vapor
275.46	1.605	1.614	water + hydrate + vapor
275.66	1.642	1.651	water + hydrate + vapor
275.86	1.682	1.690	water + hydrate + vapor
276.06	1.723	1.732	water + hydrate + vapor
276.26	1.766	1.774	water + hydrate + vapor
276.44	1.806	1.814	water + hydrate + vapor
276.64	1.846	1.855	water + hydrate + vapor
276.85	1.893	1.901	water + hydrate + vapor
277.04	1.939	1.948	water + hydrate + vapor
277.24	1.985	1.994	water + hydrate + vapor
277.43	2.035	2.044	water + hydrate + vapor
277.64	2.088	2.097	water + hydrate + vapor
277.84	2.140	2.149	water + hydrate + vapor
278.05	2.196	2.205	water + hydrate + vapor

^a Uncertainties of T and p are 0.05 K and 0.05 MPa, respectively.

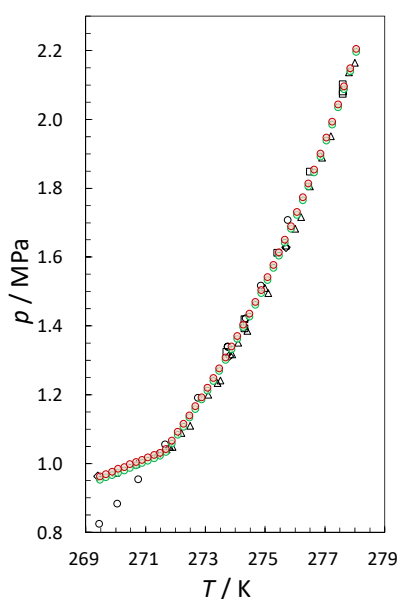


Figure 2. Three-phase (ice/water + hydrate + vapor) equilibrium p – T conditions for $^{12}\text{CO}_2$ and $^{13}\text{CO}_2$ hydrates. Green circles, $^{12}\text{CO}_2\text{-H}_2\text{O}$ (this work); brown circles, $^{13}\text{CO}_2\text{-H}_2\text{O}$ (this work); open squares, $^{12}\text{CO}_2\text{-H}_2\text{O}$ [24]; open triangles, $^{12}\text{CO}_2\text{-H}_2\text{O}$ [25]; open diamonds, $^{12}\text{CO}_2\text{-H}_2\text{O}$ [26]; open circles, $^{12}\text{CO}_2\text{-H}_2\text{O}$ [23].

Figure 3 shows the differences in $\delta^{13}\text{C}$ between the residual and hydrate-bound CO_2 ($\Delta\delta^{13}\text{C}$) in the temperature range of 226 K to 278 K. The $\delta^{13}\text{C}$ of hydrate-bound CO_2 was lower (1.0–1.5‰) than that of residual CO_2 in the temperature range used in this study. This result correlates with a previous study that reported $\sim 0.9\text{‰}$ of $\Delta\delta^{13}\text{C}$ at 268 K [17]. These results indicate that $^{12}\text{CO}_2$ molecules are preferentially encapsulated in hydrate cages as guest molecules rather than $^{13}\text{CO}_2$ molecules during the formation of CO_2 hydrates in the temperature range of 226 K to 278 K.

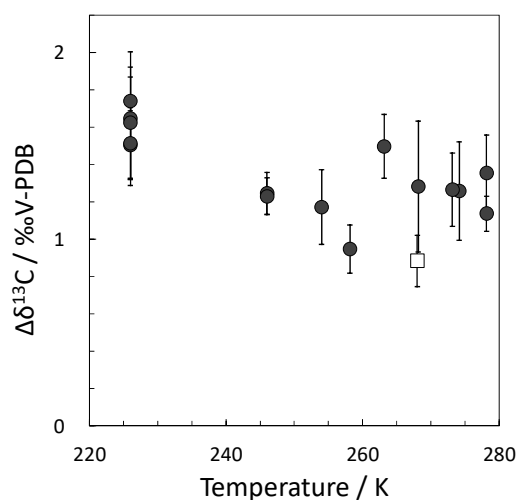


Figure 3. $\Delta\delta^{13}\text{C}$ at the formation of CO_2 hydrates that formed in the temperature range of 226–278 K. (Solid circles, this work; open square, literature) [17].

An earlier study reported hydrogen isotope fractionation in methane during the formation of methane hydrates [13]. The δD of hydrate-bound methane was $4.8 \pm 0.4\text{‰}$ lower than that of residual molecules [13]. On the other hand, the equilibrium pressures of CH_3D and CD_4 hydrates were ~ 0.04 MPa and ~ 0.14 MPa higher than those of the CH_4 hydrate, respectively [18]. For example, the equilibrium pressure of the C_2H_6 hydrate is lower than that of the CH_4 hydrate [24], resulting in a preferential C_2H_6 concentration in the hydrate phase during the formation process of CH_4 and C_2H_6 mixed-gas hydrate [24,27]. Ozeki et al. explained that the difference in equilibrium pressures between CH_3D and CH_4 hydrates causes the isotopic fractionation of hydrogen in methane during the formation of methane hydrates [18]. In this study, carbon isotope fractionation in CO_2 (the difference in $\delta^{13}\text{C}$ between the residual and hydrate gases) during the formation of CO_2 hydrates was 1.0–1.5‰ (Figure 3). As above, this trend of carbon isotope fractionation of CO_2 is reasonable because the equilibrium pressures of the $^{12}\text{CO}_2\text{--H}_2\text{O}$ system seem slightly lower than those of the $^{13}\text{CO}_2\text{--H}_2\text{O}$ system. However, it cannot be discussed here because these differences in equilibrium pressures (Table 2) are smaller than the experimental uncertainty (0.05 MPa).

3. Materials and Methods

3.1. Crystallographic Analysis

We formed fine powder samples of $^{12}\text{CO}_2$ and $^{13}\text{CO}_2$ hydrates in small pressure cells (internal volume: 8 mL). Research-grade CO_2 (purity 99.999% for CO_2 , including $\sim 1.1\%$ of $^{13}\text{CO}_2$, Takachiho Chemical Industrial) and $^{13}\text{CO}_2$ (purity 99%, Taiyo Nippon Sanso) were used as the guest $^{12}\text{CO}_2$ and $^{13}\text{CO}_2$, respectively. 1 g of fine ice powder was placed in the high-pressure cell, and the air was vacuumed at 77 K. CO_2 isotopologues were introduced to each cell and the temperature was increased from 77 K to 273.2 K to form their gas hydrates. CO_2 sublimated and increased the internal pressure. We confirmed hydrate formation by the decrease in pressure at 273.2 K. The samples were recovered and stored at 77 K for the crystallographic analysis.

PXRD measurements were performed using an X-ray diffractometer (model Ultima-III, Rigaku Co., Tokyo, Japan) with parallel beam optics and a low-temperature chamber. Finely-powdered hydrate samples were mounted on a PXRD sample holder made of 2.5 mm thick Cu at 93 K. Each measurement was performed in a $\theta/2\theta$ step scan mode with a step width of 0.02° using Cu $\text{K}\alpha$ radiation ($\lambda = 1.541 \text{ \AA}$).

We obtained the Raman spectra of $^{12}\text{CO}_2$ and $^{13}\text{CO}_2$ hydrates. A Raman spectrometer (RMP-210, Jasco Co., Tokyo, Japan) was used equipped with a 532 nm excitation source

(100 mW), a single holographic diffraction grating (1800 grooves per mm), and a charged coupled device detector. The spectrum pixel resolution, which is the spectrum's sampling interval, was 1.1 cm^{-1} per pixel in the range of $1200\text{--}1400\text{ cm}^{-1}$. The wavenumber was calibrated using atomic emission lines from a neon lamp. The Raman spectra for the C–O symmetric stretch region ($1200\text{--}1400\text{ cm}^{-1}$) of the encapsulated CO_2 molecules in the gas hydrate water cages were obtained at ambient pressure and 140 K using a cooling stage (THMS600, Linkam Scientific Instruments Ltd., Tadworth, UK). The peak positions could be rigorously analyzed by fitting the data to a Voigt function, allowing us to obtain high positional accuracy.

3.2. Measurement for Equilibrium Pressure

To obtain the data of equilibrium pressures of $^{12}\text{CO}_2$ and $^{13}\text{CO}_2$ hydrates, we formed them in the same small pressure cells as those used for crystallographic analysis. The experimental setup to achieve their equilibrium condition was described in [18]. 1 g of fine ice powder was placed in the cell, evacuated at 77 K, and CO_2 isotopologues were introduced in the amount needed to achieve equilibrium conditions of the ice/liquid water, hydrates, and vapor at $\sim 273.2\text{ K}$. The hydrate-enclathrated CO_2 isotopologues were formed by melting the ice powder at 273.2 K under high pressure of CO_2 . The decrease in pressure due to hydrate formation was observed at 273.2 K.

The equilibrium hydrate dissociation and formation conditions were determined using a phased isochoric method of heating and cooling [18]. Three-phase (ice/water + hydrate + vapor) equilibrium conditions were achieved by increasing the temperature by 0.4 K and then decreasing it by 0.2 K. Since two values of equilibrium pressure at each temperature by heating and cooling were obtained, we determined the phase equilibrium points as their average temperatures and pressures. The phase equilibrium data of $^{12}\text{CO}_2$ and $^{13}\text{CO}_2$ hydrates were obtained between 269 K and 278 K. The uncertainties of the temperature and pressure measurements were 0.05 K and 0.05 MPa, respectively.

3.3. Gas Analysis for Detecting Carbon Isotope Fractionation

The preparation method of gas hydrate samples for measuring isotopic fractionation was the same as that of [13]. Research-grade CO_2 gas was used as the guest gas (purity 99.999% for CO_2 , including $\sim 1.1\%$ of $^{13}\text{CO}_2$, Takachiho Chemical Industrial). Distilled and deionized water was used as host molecules. The temperature effect on isotope fractionation was confirmed by forming CO_2 hydrate samples at 226 K, 246 K, 254 K, 258 K, 263 K, 268 K, 273 K, 274 K, and 278 K. For the samples formed below the freezing point of water, fine ice powder (0.7 g) was filled in a high-pressure cell (internal volume: 42 mL) in a cold room at 253 K. For the samples formed above the freezing point of water, 5 g water was filled into a high-pressure cell equipped with a stirring device (internal volume: 150 mL). These high-pressure cells were cooled to below 90 K, vacuumed inside the air, and CO_2 was introduced into the cell. The amount of CO_2 was controlled to reach above the equilibrium pressure of CO_2 hydrates and below the CO_2 liquefaction pressure at each temperature. These cells were set into a circulating constant-temperature bath ($>255\text{ K}$) or cold rooms (226 K and 246 K) to maintain each temperature for hydrate formation. The trapped CO_2 in the cells sublimated and reached the desired pressure at each temperature. The internal pressure decreased as the CO_2 hydrates formed. When the pressure stabilized and the pressure decrease rate was lower than 0.01 MPa h^{-1} , the residual gas that was not encapsulated in the gas hydrate was collected. The cell was cooled below 90 K and the hydrate sample was recovered from the cell. The residual and hydrate-bound gases were retrieved in a vacuum line system and their pressures were adjusted to atmospheric pressure.

Each gas sample was introduced into a continuous-flow isotope ratio mass spectrometer (CF-IRMS, Delta V, Thermo Fisher Scientific Inc., Waltham, MA, USA) coupled with a gas chromatograph (TRACE GC Ultra, Thermo Fisher Scientific Inc., Waltham, MA, USA) using a syringe injection. The gas chromatograph was equipped with a CP-PoraPLOT Q

capillary column (length 25 m, ID 0.32 mm, film thickness 10 μm , Agilent Technologies). Carbon isotope compositions were reported as δ values (‰),

$$\delta [\text{‰}] = \left(\frac{R_{\text{sample}} - R_{\text{standard}}}{R_{\text{standard}}} \right) \times 1000 \quad (1)$$

where R denotes the $^{13}\text{C}/^{12}\text{C}$ ratio. $\delta^{13}\text{C}$ is given referring to the V-PDB standards, determined using NIST RM8544 (NBS19). The analytical precision was 0.1‰. The difference between the $\delta^{13}\text{C}$ of the hydrate-bound gas and that of the residual gas was determined ($\delta^{13}\text{C}$ of the residual gas – $\delta^{13}\text{C}$ of the hydrate-bound gas, defined as $\Delta\delta^{13}\text{C}$).

4. Conclusions

We synthesized isotopologue CO_2 hydrates to obtain their crystallographic properties. From the Raman spectra of $^{12}\text{CO}_2$ and $^{13}\text{CO}_2$ hydrates, definite differences were found in the Raman shift of Fermi dyad of $^{12}\text{CO}_2$ and $^{13}\text{CO}_2$ encapsulated in hydrate cages, although their unit cell size was similar. We investigated carbon isotope fractionation during the formation of CO_2 hydrates and measured the three-phase equilibria of $^{12}\text{CO}_2\text{-H}_2\text{O}$ and $^{13}\text{CO}_2\text{-H}_2\text{O}$ systems. The $\delta^{13}\text{C}$ of hydrate-bound CO_2 was lower than that of the residual CO_2 (1.0–1.5‰) in the formation temperature range between 226 K to 278 K. From the results of isotopic fractionation, differences in equilibrium pressures were expected. The equilibrium pressures in the $^{12}\text{CO}_2\text{-H}_2\text{O}$ system were slightly lower by 0.007–0.012 MPa compared with the corresponding values in the $^{13}\text{CO}_2\text{-H}_2\text{O}$ system between 269 K to 278 K. We concluded that the small difference in equilibrium pressures of ~ 0.01 MPa between $^{12}\text{CO}_2$ and $^{13}\text{CO}_2$ hydrates causes carbon isotope fractionation of 1.0–1.5‰. However, the pressure differences obtained were within the range of the uncertainty of the pressure measurements. More accurate measurements of equilibrium pressure are needed for further discussion. These results caused by carbon isotope fractionation will be useful for a better understanding of the formation and dissociation of naturally occurring CO_2 hydrates.

Supplementary Materials: The following is available online: Figure S1, Powder X-ray diffraction patterns of the hydrate enclathrated CO_2 isotopologues.

Author Contributions: H.K. prepared the samples, analyzed the gas data, and conducted Raman spectroscopy; G.F. wrote the draft of paper; S.T. conducted the PXRD analysis; and A.H. designed the experiments and supervised this project. All authors commented on and approved the paper. All authors have read and agreed to the published version of the manuscript.

Funding: Gas measuring system in this research was funded by the Japan Society for the Promotion of Science KAKENHI 26303021.

Institutional Review Board Statement: Not applicable.

Informed Consent Statement: Not applicable.

Data Availability Statement: Available from the authors.

Acknowledgments: The authors gratefully acknowledge Jumpei Matsuda and Yuki Kikuchi for their technical support during the experiments.

Conflicts of Interest: The authors declare no conflict of interest.

Sample Availability: Samples of the compounds are not available from the authors.

References

1. Sloan, E.D.; Koh, C.A. *Clathrate Hydrates of Natural Gases*, 3rd ed.; CRC Press Taylor and Francis Group: Boca Raton, FL, USA, 2008.
2. Sluijs, A.; Brinkhuis, H.; Schouten, S.; Bohaty, S.M.; John, C.M.; Zachos, J.C.; Reichart, G.-J.; Sinninghe Damsté, J.S.; Crouch, E.M.; Dickens, G.R. Environmental precursors to rapid light carbon injection at the Palaeocene/Eocene boundary. *Nature* **2007**, *450*, 1218–1221. [[CrossRef](#)]
3. Kennedy, M.; Mrofka, D.; Von Der Borch, C. Snowball Earth termination by destabilization of equatorial permafrost methane clathrate. *Nature* **2008**, *453*, 642–645. [[CrossRef](#)]

4. Ménot, G.; Bard, E. Geochemical evidence for a large methane release during the last deglaciation from Marmara Sea sediments. *Geochim. Cosmochim. Acta* **2010**, *74*, 1537–1550. [[CrossRef](#)]
5. Shipley, T.H.; Didyk, B.M. Occurrence of methane hydrates offshore southern Mexico. In *Initial Reports of the Deep Sea Drilling Project*; Watkins, J.S., Moore, J.C., Eds.; USA Govt Printing Office: Washington, DC, USA, 1982; Volume 66, pp. 547–555.
6. Brooks, J.M.; Kennicutt, M.C., II; Fay, R.R.; McDonald, T.J.; Sassen, R. Thermogenic gas hydrates in the Gulf of Mexico. *Science* **1984**, *225*, 409–411. [[CrossRef](#)]
7. Jin, Y.; Kida, M.; Yoneda, J.; Konno, Y.; Oshima, M.; Tenma, N.; Nagao, J. Natural gas hydrates recovered from the Umitaka Spur in the Joetsu Basin, Japan: Coexistence of two structure-I hydrates with distinctly different textures and gas compositions within a massive structure. *ACS Earth Space Chem.* **2020**, *4*, 77–85. [[CrossRef](#)]
8. Sakai, H.; Gamo, T.; Kim, E.-S.; Tsutsumi, M.; Tanaka, T.; Ishibashi, J.; Wakita, H.; Yamano, M.; Oomori, T. Venting of carbon dioxide-rich fluid and hydrate formation in Mid-Okinawa Trough Backarc Basin. *Science* **1990**, *248*, 1093–1096. [[CrossRef](#)]
9. Lupton, J.; Butterfield, D.; Lilley, M.; Evans, L.; Nakamura, K.; Chadwick, W., Jr.; Resing, J.; Embley, R.; Olson, E.; Proskurowski, G.; et al. Submarine venting of liquid carbon dioxide on a Mariana Arc volcano. *Geochem. Geophys. Geosyst.* **2006**, *7*, Q08007. [[CrossRef](#)]
10. Miller, S.L.; Smythe, W.D. Carbon dioxide clathrate in the Martian ice cap. *Science* **1970**, *170*, 531–533. [[CrossRef](#)]
11. Dobrovolskis, A.; Ingersoll, A.P. Carbon dioxide-water clathrate as a reservoir of CO₂ on Mars. *Icarus* **1975**, *26*, 353–357. [[CrossRef](#)]
12. Ambuehl, D.; Madden, M.E. CO₂ hydrate formation and dissociation rates: Application to Mars. *Icarus* **2014**, *234*, 45–52. [[CrossRef](#)]
13. Hachikubo, A.; Kosaka, T.; Kida, M.; Krylov, A.; Sakagami, H.; Minami, H.; Takahashi, N.; Shoji, H. Isotopic fractionation of methane and ethane hydrates between gas and hydrate phases. *Geophys. Res. Lett.* **2007**, *34*, L21502. [[CrossRef](#)]
14. Hachikubo, A.; Khlystov, O.; Manakov, A.; Kida, M.; Krylov, A.; Sakagami, H.; Minami, H.; Takahashi, N.; Shoji, H.; Kalmychkov, G.; et al. Model of formation of double structure gas hydrates in Lake Baikal based on isotopic data. *Geophys. Res. Lett.* **2009**, *36*, L18504. [[CrossRef](#)]
15. Hachikubo, A.; Krylov, A.; Sakagami, H.; Minami, H.; Nunokawa, Y.; Shoji, H.; Matveeva, T.; Jin, Y.K.; Obzhairov, A. Isotopic composition of gas hydrates in subsurface sediments from offshore Sakhalin Island, Sea of Okhotsk. *Geo-Mar. Lett.* **2010**, *30*, 313–319. [[CrossRef](#)]
16. Hachikubo, A.; Minami, H.; Yamashita, S.; Khabuev, A.; Krylov, A.; Kalmychkov, G.; Poort, J.; De Batist, M.; Chenskiy, A.; Manakov, A.; et al. Characteristics of hydrate-bound gas retrieved at the Kedr mud volcano (southern Lake Baikal). *Sci. Rep.* **2020**, *10*, 14747. [[CrossRef](#)]
17. Luzi, M.; Schicks, J.M.; Erzinger, J. Carbon isotopic fractionation of synthetic methane and carbon dioxide hydrates. In Proceedings of the 7th International Conference on Gas Hydrates (ICGH2011), Edinburgh, UK, 17–21 July 2011.
18. Ozeki, T.; Kikuchi, Y.; Takeya, S.; Hachikubo, A. Phase equilibrium of isotopologue methane hydrates enclathrated CH₃D and CD₄. *J. Chem. Eng. Data* **2018**, *63*, 2266–2270. [[CrossRef](#)]
19. Nakano, S.; Moritoki, M.; Ohgaki, K. High-pressure phase equilibrium and Raman microprobe spectroscopic studies on the CO₂ hydrate system. *J. Chem. Eng. Data* **1998**, *43*, 807–810. [[CrossRef](#)]
20. Kumar, R.; Englezos, P.; Moudrakovski, I.; Ripmeester, J.A. Structure and composition of CO₂/H₂ and CO₂/H₂/C₃H₈ hydrate in relation to simultaneous CO₂ capture and H₂ production. *AIChE J.* **2009**, *55*, 1584–1594. [[CrossRef](#)]
21. Qin, J.; Kuhs, W.F. Quantitative analysis of gas hydrates using Raman spectroscopy. *AIChE J.* **2013**, *59*, 2155–2167. [[CrossRef](#)]
22. Shimanouchi, T. *Tables of Molecular Vibrational Frequencies, Consolidated Volume I*; US Government Printing Office: Washington, DC, USA, 1972; p. 39.
23. Nema, Y.; Ohmura, R.; Senaha, I.; Yasuda, K. Quadruple point determination in carbon dioxide hydrate forming system. *Fluid Phase Equilib.* **2017**, *441*, 49–53. [[CrossRef](#)]
24. Deaton, W.M.; Frost, E.M. *Gas Hydrates and Their Relation to the Operation of Natural-Gas Pipe Lines*; American Gas Association: Washington, DC, USA, 1946; Volume 8.
25. Larson, S.D. Phase Studies of the Two-Component Carbon Dioxide-Water System, Involving the Carbon Dioxide Hydrate. Ph.D. Thesis, University of Illinois, Urbana, IL, USA, 1955.
26. Yasuda, K.; Ohmura, R. Phase equilibrium for clathrate hydrates formed with methane, ethane, propane, or carbon dioxide at temperatures below the freezing point of water. *J. Chem. Eng. Data* **2008**, *53*, 2182–2188. [[CrossRef](#)]
27. Hachikubo, A.; Kida, M.; Okuda, M.; Sakagami, H.; Shoji, H. Dissociation heat of mixed-gas hydrate composed of methane and ethane. *Seppyo* **2009**, *71*, 341–351.